




Article

New Insights into Flexible Transparent Conductive Silver Nanowires Films

Yuehui Wang ^{1,*} , Xing Yang ², Dexi Du ², Yuzhen Zhao ³ and Xianfeng Zhang ^{1,*}

¹ Department of Materials and Food, University of Electronic Science and Technology of China Zhongshan Institute, Zhongshan 528402, China

² School of Materials and Energy, University of Electronic Science and Technology of China, Chengdu 610054, China; shirleywyh@126.com (X.Y.); dudexi_work@foxmail.com (D.D.)

³ Department of Materials Science and Engineering, Tsinghua University, Beijing 100084, China; zhaoyz@mail.tsinghua.edu.cn

* Correspondence: wangzsedu@126.com (Y.W.); zhangxf07@gmail.com (X.Z.); Tel.: +86-159-0002-0061 (Y.W.)

Received: 26 April 2019; Accepted: 30 May 2019; Published: 8 June 2019



Abstract: Flexible transparent conductive films (FTCFs) composed of silver nanowires (AgNWs) have become an important research direction because of their potential in flexible electronic devices. The optoelectronic properties of FTCFs composed of AgNWs of different lengths were evaluated in this study. AgNWs, with an average diameter of about 25 nm and length of 15.49–3.92 μm were obtained by a sonication-induced scission process. AgNW-FTCFs were prepared on polyethylene terephthalate substrates using a Meyer bar and then dried in the ambient environment. The sheet resistance, non-uniformity factor of the sheet resistance, the root mean square roughness, and haze of the FTCFs increased as the length of AgNWs decreased. The transmittance of the films increased slightly as the length of AgNWs increased. AgNWs with a length of 15.49 μm provided an AgNW-FTCF with excellent properties including haze of 0.95%, transmittance of 93.42%, and sheet resistance of 80.15 $\Omega\cdot\text{sq}^{-1}$, without any additional post-treatment of the film. This work investigating the dependence of the optoelectronic properties of AgNW-FTCFs on AgNW length provides design guidelines for development of AgNW-FTCFs.

Keywords: silver nanowire; flexible transparent conductive film; sonication-induced scission; haze

1. Introduction

As the demand for flexible and wearable electronic devices has increased over the last 20 years, the development of the flexible transparent conducting films (FTCFs) with excellent electrical conductivity, flexibility, and optical transparency has become important. At present, indium tin oxide (ITO) is a widely used material for the transparent conducting films; however, because of its intrinsic brittleness, relative rarity, and expensive deposition and post-treatment processes, ITO is not suitable for flexible device fabrication. To circumvent the shortcomings of ITO, many materials, including carbon nanotubes [1,2], graphene [3,4], and metal nanowires [5,6], have been studied to find appropriate materials for use as FTCFs.

Silver nanowire (AgNW) films have excellent optical and electrical properties comparable to that of ITO and are regarded as a leading candidate for FTCFs [5–8]. The properties of AgNW-FTCFs makes them attractive for usage in FTCTF wearable devices, organic light emitting diodes, displays, heaters, and other flexible electronics applications [9–15]. An AgNW-FTCF contains a percolation network consisting of randomly distributed and overlapped AgNWs. The conductive networks of AgNW-FTCFs are only composed of AgNWs and pores, and several studies have indicated that the properties of AgNW-FTCFs are defined mainly by the size, aspect ratio, and purity of AgNWs,

contact between AgNWs and network morphology [16–18]. Longer AgNWs may form a network with longer conducting paths, lower deposition density and a decreased number of junctions between AgNWs, which lowers junction resistance. These factors indicate that longer AgNWs can improve the conductivity of FTCFs. Meanwhile, thinner AgNWs decrease the deposition area and light scattering, improving the optical transparency and haze of FTCFs [19,20]. The high aspect ratio of AgNWs enables electrical percolation without covering the whole substrate surface [19,20]. However, the large-scale synthesis of AgNWs with long length and small diameter is still difficult.

Generally, it is challenging to fabricate a high-performance AgNWs film with both high transmittance and high electrical conductivity, because AgNWs are not transparent. Meanwhile, the haze of AgNW-FTCFs strongly depends on the diameter of AgNWs and is decreased by using AgNWs with a smaller diameter [19–21]. High uniformity and low haze are two importance factors for high-end applications of the AgNWs–FTCFs. However, the reported haze and uniformity of such films are still bottlenecks in current research. Chen et al. [22] prepared FTCFs using highly purified AgNWs and achieved a remarkably low haze of 0.8% and a small sheet resistance non-uniformity factor of 5.0% at $71.2 \Omega \cdot \text{sq}^{-1}$. Bergin et al. recently reported that the transmittance of AgNW-FTCFs with AgNWs of a given diameter is linearly to area coverage, and does not depend on the length of the AgNWs. In addition, they found that decreasing AgNWs diameter improved optoelectronic performance only for AgNWs with a diameter of less than 20 nm [23]. Sorel et al. measured the transmittance and sheet resistance for a large number of networks of AgNWs with different lengths and diameters [24]. They found that the network direct current conductivity scaled linearly with wire length, whereas the optical conductivity remained approximately constant regardless of nanowire length. Many studies have focused on controlling the topology of AgNWs networks and AgNWs distributions [25–28]. However, very few systematic experimental studies have evaluated the relationship between the electro-optical properties and microstructure of AgNW-FTCFs.

Herein, we produce AgNWs with different lengths by a sonication-induced scission process and explained relationship of the length of AgNWs with ultrasonic time and then fabricate FTCFs composed of the AgNWs of different lengths. Furthermore, the influence of AgNWs length on the sheet resistance, non-uniformity factor of the sheet resistance, transmittance, haze, and root mean square roughness of AgNW-FTCFs were discussed in a systemic way. In addition, the relationship of the optoelectronic properties of film with microstructures was discussed. The uniformity of the AgNWs networks decreases with decreasing of AgNWs length. The resulting FTCF composed of $15.5 \mu\text{m}$ AgNWs has high transparency, low sheet resistance and haze and root mean square roughness, and high uniformity. We would like to point out that the AgNW-FTCFs conductive film prepared have no any additional post-treatment.

2. Results and Discussion

2.1. Sonication-Induced Scission of Silver Nanowires

Figure 1a,b shows SEM images of the commercial AgNWs. The average length and diameter of the AgNWs were 25 nm and $15.49 \mu\text{m}$, respectively. SEM images of the AgNWs ($1.7 \text{ mg} \cdot \text{mL}^{-1}$) after sonication-induced scission at an ultrasonic power of 300 W for $0.5, 1.0, 1.5, 2.0, 2.5,$ and 3.0 h , are presented in Figure 2. The inserted images display the length distribution of AgNWs in each sample. After $0.5, 1.0, 1.5, 2.0, 2.5,$ and 3.0 h of ultrasonic treatment, the length of the AgNWs decreased from $15.5 \mu\text{m}$ before treatment to $9.48, 9.24, 8.95, 7.86, 5.17,$ and $3.92 \mu\text{m}$, respectively. AgNW scission was attributed to the sonication energy [29]. However, the change in the AgNWs diameter was not observed. The length distributions of sonicated AgNWs were considerably narrower than that of the initial length distribution of AgNWs, indicating that the long AgNWs were fragmented during ultrasonication and short AgNWs were not. This results suggestion that the decrease in AgNW length is dominated by a mechanical shearing process resulting from the fluid flow [29,30]. The length of AgNWs during sonication-induced scission decreased obviously within the first 0.5 h , over the next

2 h, the length of the AgNWs gradually decreased. The reason for this behavior is that shorter AgNWs can be dragged away more easily by the fluid flow than longer AgNWs [29].

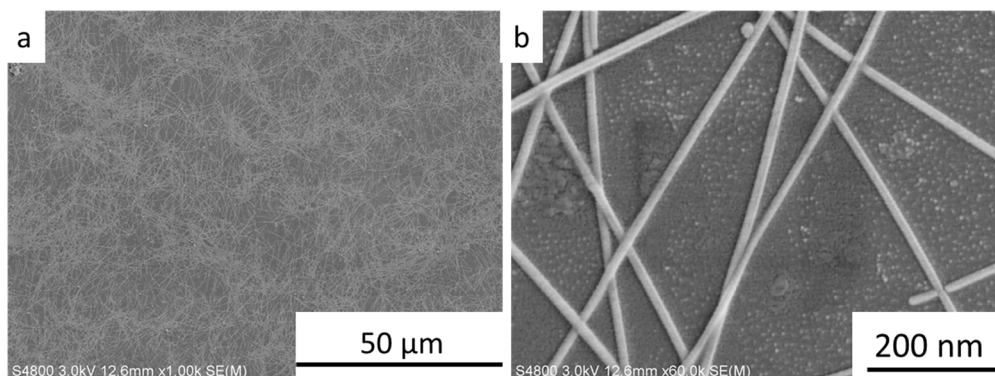


Figure 1. SEM images of commercial AgNWs at low (a) and high (b) magnification.

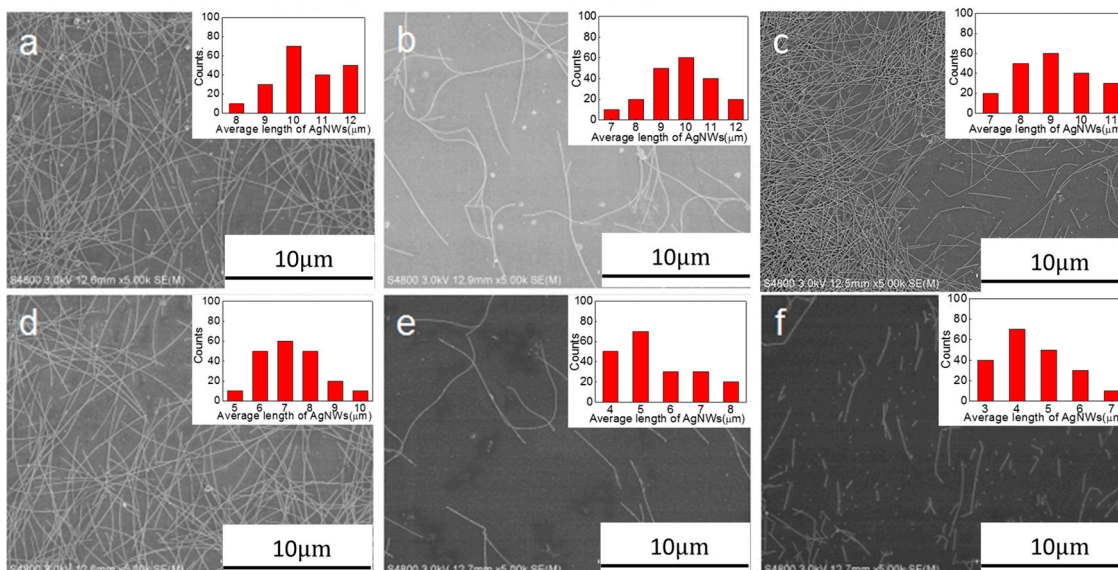


Figure 2. SEM images of AgNWs subjected to sonication-induced scission at an ultrasonic power of 300 W for (a) 0.5, (b) 1.0, (c) 1.5, (d) 2.0, (e) 2.5, and (f) 3 h. Insets show the corresponding AgNWs length distributions.

Figure 3 shows the relationship between the average length of AgNWs and ultrasonic treatment time. By fitting the data points, we obtained the linear function between the average length of the AgNWs and ultrasonic treatment time, shown in Equation (1):

$$1/L = 0.0548t + 0.0558, R^2 = 0.8418 \tag{1}$$

where t is the ultrasonic time and $L(t)$ represents the average length of AgNWs at a certain t . The ultrasonic energy at constant ultrasonic power is proportional to the ultrasonic treatment time.

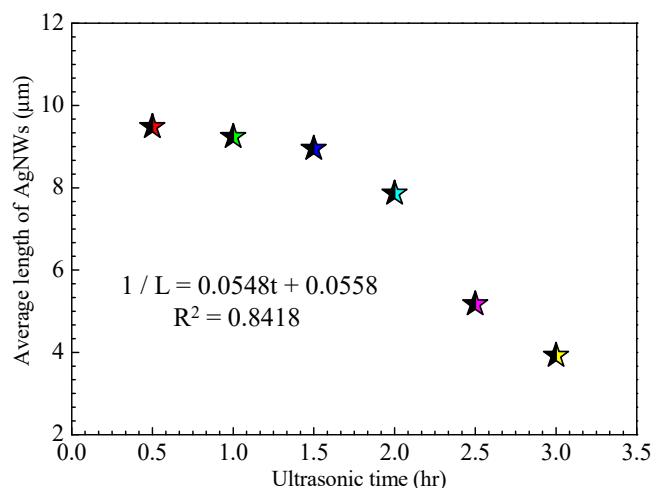


Figure 3. Relationship between the average length of AgNWs and ultrasonic treatment time.

2.2. Flexible Transparent Conductive Films of Silver Nanowires

Conductive films consisting of AgNWs of different lengths were fabricated on polyethylene terephthalate (PET) substrates using a Mayer rod. A schematic diagram of the fabrication of an AgNW-FTCF is shown in Figure 4. Conductivity and the uniformity of conductivity of AgNW-FTCFs are important factors for evaluating the performance. Jia et al. defined a non-uniformity factor (*NUF*) to evaluate the standard deviation of the sheet resistance of the films from the average value as follows [31]:

$$NUF = \sqrt{\frac{\sum_{i=1}^n (R_i - \bar{R})^2}{n\bar{R}^2}} \quad (2)$$

where *n* is the number of measurements of the film of different sites, and R_i and \bar{R} are the measured resistance and average resistance for all the measurements, respectively. The smaller *NUF*, the more uniform the film. According to this method, we divided film into 64 regions of the same size, measured the sheet resistance of each region and recorded the data.

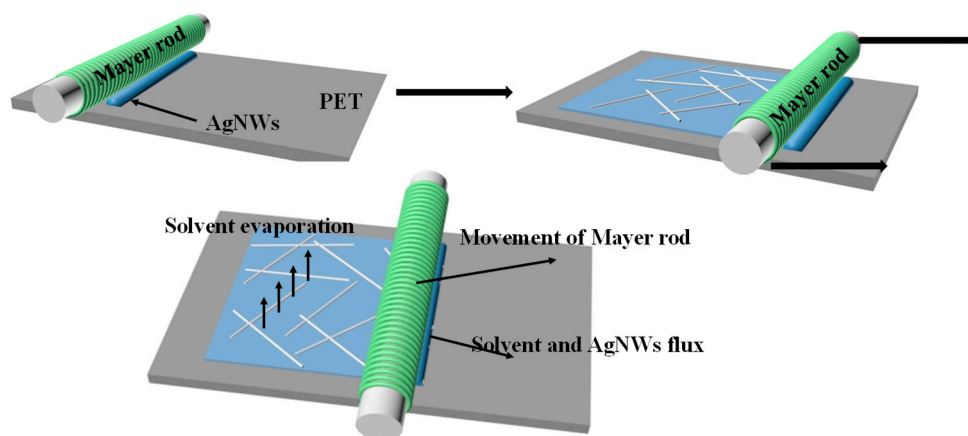


Figure 4. Schematic diagram illustrating the fabrication of an AgNW-flexible transparent conducting films (FTCF) using the Mayer rod method.

Figure 5 presents the sheet resistance and *NUF* of the sheet resistance of films consisting of AgNWs of different lengths. Results for the films containing AgNWs with average lengths of 5.17 and 3.92 μm are not shown in Figure 5 because these films were not conductive. The sheet resistance of the lengths of AgNW-FTCFs with AgNW lengths of 15.49, 9.48, 9.24, 8.95, and 7.86 μm were 80.15,

130.23, 273.46, 543.23, and 5130 $\Omega \cdot \text{sq}^{-1}$, respectively. As the length of the AgNWs decreased from 15.5 to 7.86 μm , the sheet resistance of the film increases by about 6400%. As the length of the AgNWs in the AgNW-FTCFs decreased from 15.5 to 7.86 μm , *NUF* rose from 0.29 to 0.52, indicating that the distribution uniformity of AgNWs on the PET surface decreased. As the distribution uniformity of AgNWs decreases, it is difficult to AgNWs to form continuous and effective conductive paths in all direction of our films were considerably smaller than those reported in the literature [32,33], indicating that our AgNW-FTCFs have good uniformity.

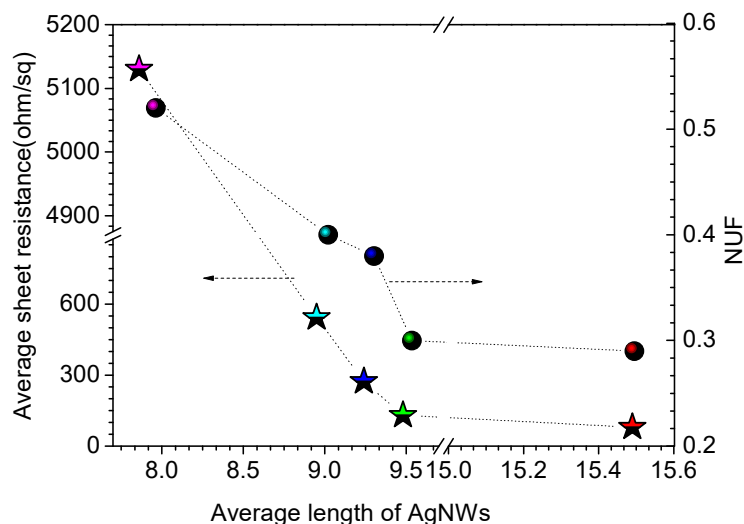


Figure 5. Sheet resistance and non-uniformity factor (*NUF*) of the sheet resistance of films consisting of AgNWs of different lengths.

Transmittance spectra and the transmittance values at a wavelength of 550 nm of the AgNW-FTCFs containing AgNWs of different lengths are depicted in Figure 6a and b, respectively. The inset in Figure 6a contains photographs of the films. AgNW-FTCFs containing AgNWs with lengths of 15.5, 9.48, 9.24, 8.95, and 7.86 μm , displayed the transmittance values at 550 nm of 93.42%, 92.97%, 92.80%, 92.28%, and 91.99%, respectively. These values show that the transmittance decreases slightly as the length of AgNWs shortens. Comparison with Figure 5 reveals that the influence of AgNWs length on film conductivity is much greater than that on optical transparency

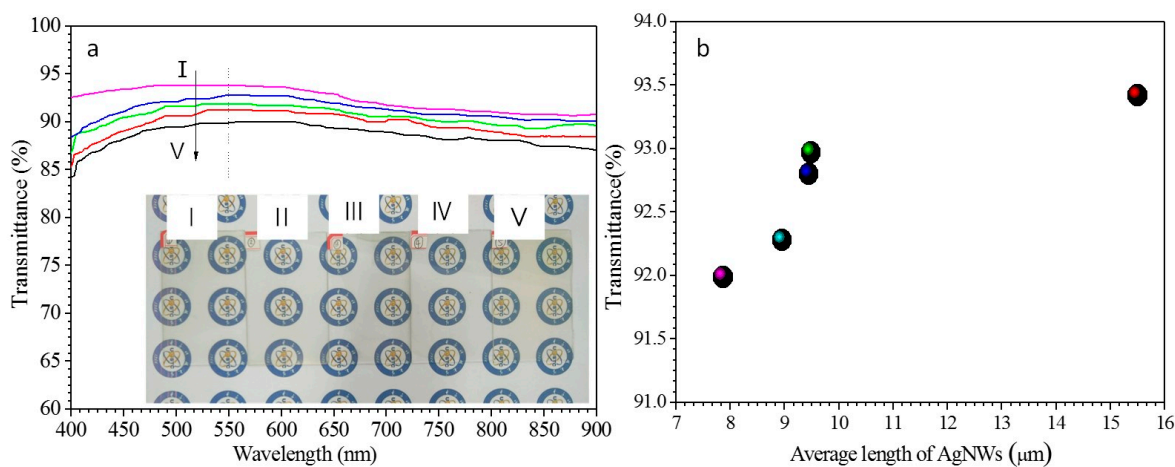


Figure 6. Transmittance (a) and transmittance at 550 nm (b) of AgNWs films consisting of the different lengths of AgNWs. The inset in (a) from I to V contains photographs of the films composed with AgNWs lengths of 15.5, 9.48, 9.24, 8.95, and 7.86 μm , respectively.

SEM analysis provided an explanation for the influences of AgNW length of on the optical and electric performances of the AgNWs films. Figure 7 reveals that with decreasing AgNW length, the uniformity of the AgNWs distribution decreased, which might be a partial removal of PVP that leads to agglomeration of AgNWs. AgNWs with length of 15.5 μm (Figure 7a) and 9.48 μm (Figure 7b) formed continuous networks that with multiple overlapping junctions between different nanowires; the nanowires within the network were randomly or almost randomly arranged, and evenly distributed on the PET surface. Conversely, when the AgNWs with a length of 7.86 μm formed a discontinuous network on PET surface, which lead to the poor electrical conductivity of this film.

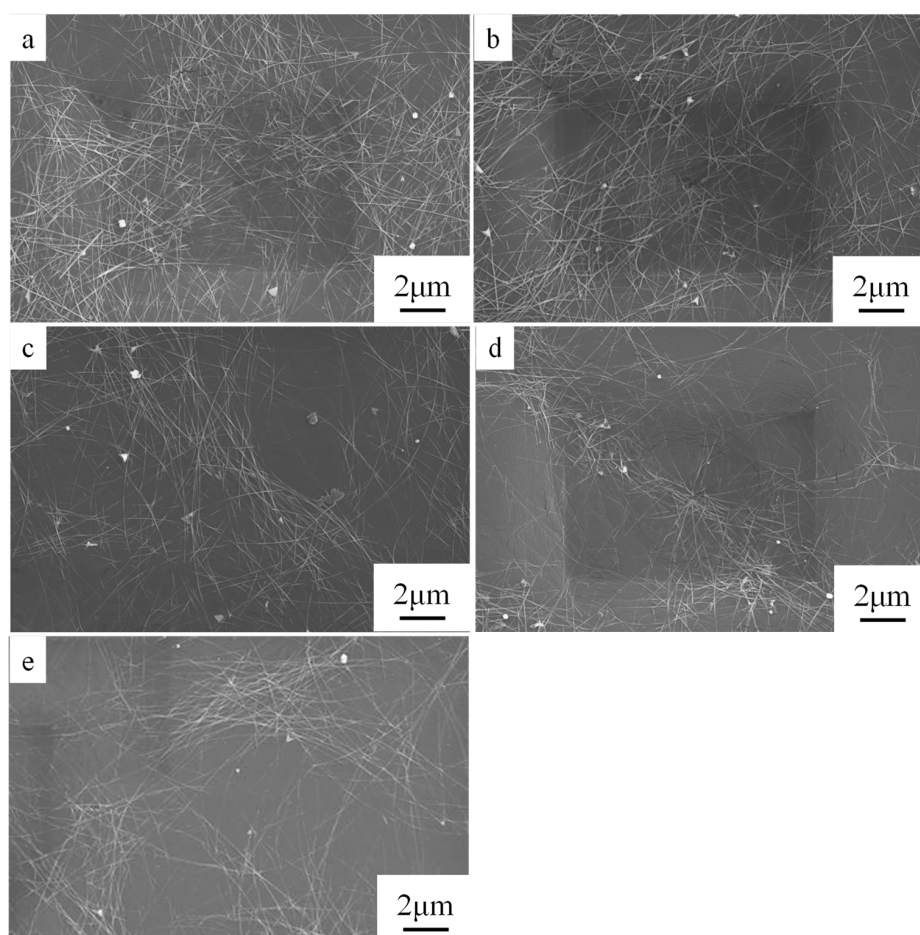


Figure 7. SEM images of AgNW films consisting of AgNWs with length of (a) 15.5 μm , (b) 9.48 μm , (c) 9.24 μm , (d) 8.95 μm , and (e) 7.86 μm .

Tighter contact between crossed AgNWs resulted in higher conductivity; the long AgNWs in the network provided multiple electrical pathways from one edge of the network to the other, which meant that breaking a relatively small number of junctions would still leave alternative electrical paths from one edge of the network to the other. However, when the length of AgNWs and the distribution uniformity decrease, the discontinuous AgNWs networks are formed and the contact resistance increased considerably, resulting in a substantial decrease of electrical conductivity. In addition, for the theoretical sticks with a given length (L) that are widthness in two dimensions, the critical number density (N_C) of sticks required for percolation is given by Equation (3) [34,35]:

$$N_C \times L^2 = 5.71 \quad (3)$$

Equation (3) indicates that the N_C of AgNWs required to form a percolation network is inversely proportional to the square of L . Therefore, a low number density of long AgNWs can form a sparse and

effective percolation network. Such a network can not only increase the light transmission, but also improve conductivity forming long percolation routes with few nanowire junctions. Figure 8 illustrates the effect of AgNW length on network connectivity and thus optoelectronic properties of the AgNW films. R_i is the internal resistance of AgNW and R_c is the contact resistance between AgNWs. The total resistance of the conductive film can be regarded as the sum of R_i and R_c , where R_c can be considered equivalent to the concentrated resistance, which is the resistance produced when the current flows through a very small conductive contact point and is compressed by convergence. For network structures composed of AgNWs, the number of contact points between AgNWs obviously depends on AgNW lengths. A junction resistance always exists between AgNWs. The higher the number of contact points, the higher the junction resistance in an AgNW network. In general, a typical AgNW-FTCF shows low conductivity because the AgNWs network contains numerous contact points, which leads to high junction resistance. For films composed of long AgNWs, the junction resistance is low because of the limited number of contact points. Conversely, for film composed of short AgNWs, the junction resistance is high because of the numerous contact points. This indicates that minimizing the junction resistance was important to obtain AgNW-FTCFs with high conductivity without post-treatment.

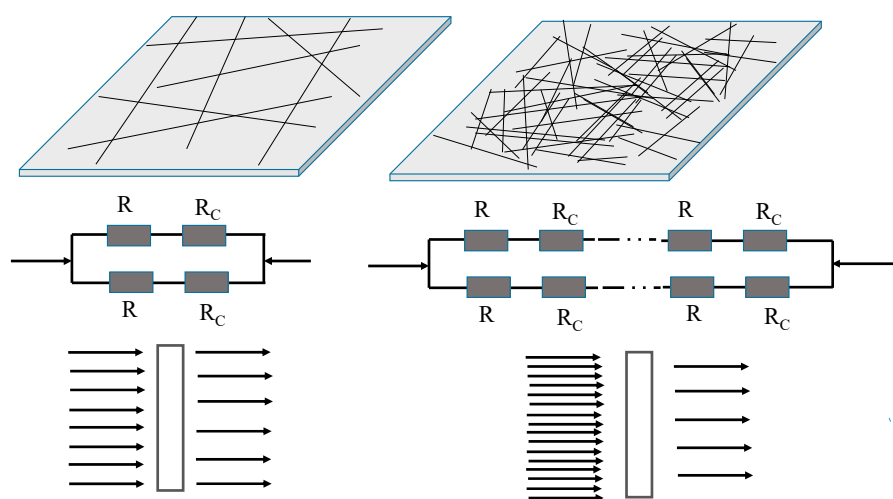


Figure 8. Schematic diagram of the relationship between the AgNWs length and optoelectronic properties of their thin films.

For a given concentration of AgNWs, decreasing the length of AgNWs increases the number, which results in increased contact resistance of their film. In addition, with the decreasing AgNW lengths, the distribution uniformity of AgNWs on the substrate surface decreased, resulting in difficulty forming an effective conductive network between AgNWs, which increased the film resistance. Meanwhile, increasing the number of AgNWs increased their deposition density on the substrate, which decreased the transmittance. The effect of AgNW length on optoelectronic properties is especially important at high transmittance (low area coverage), where there are relatively few connections between nanowires, i.e., the film is porous.

In general, figure of merit (FoM) is defined the ratio σ_{DC}/σ_{Op} , where σ_{Op} (λ) is the optical conductivity and σ_{DC} is the direct current (DC) conductivity of the film, which is one of the important parameters for evaluating the optoelectronic properties of optoelectronic films. Here, we calculated FoM of the film, as shown in Figure 9. As can be seen from Figure 9, with decreasing of AgNW length, FoM decreased gradually. When the AgNW length decreased from 15.5 m to 7.86 m, the film FoM decreased from 67.9 to 0.86, which was reduced by about 790%. This result indicated that the AgNW length has great influence on optoelectronic properties of film. As we know that transparent conductive film as electrode to be used in optoelectronic devices, the σ_{DC}/σ_{Op} value is at least 35, which corresponds to the resistance sheet less than 100 Ω with a transmittance at 550 nm over 90%, meanwhile, σ_{DC}/σ_{Op} values of film need over 50 and 10 when they are used in liquid crystal display

and touch screen panels, respectively [36]. We would like to point out that the AgNW conductive film prepared in our lab is suitable for the above applications, especially for the display screen due to the low haze.

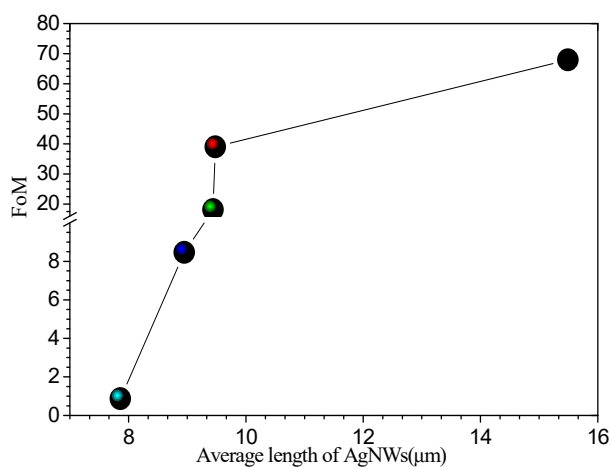


Figure 9. Relationship between figure of merit (FoM) of AgNW-FTCFs and the average AgNW length.

To further study the effect of AgNW length on morphology, the films with AgNW lengths of 15.5, 9.24, and 7.86 μm were analyzed by AFM as shown in Figure 10. The measured root mean square roughness (RMS) values of the film with AgNW lengths of 15.5, 9.24, and 7.86 μm were 12.9, 18.4, and 22.3 nm, respectively. These RMS values are low approximately the diameter of a nanowire. The RMS values of the films increases with decreasing AgNW length, which may be related to the non-uniform distribution and high local deposition density of AgNWs.

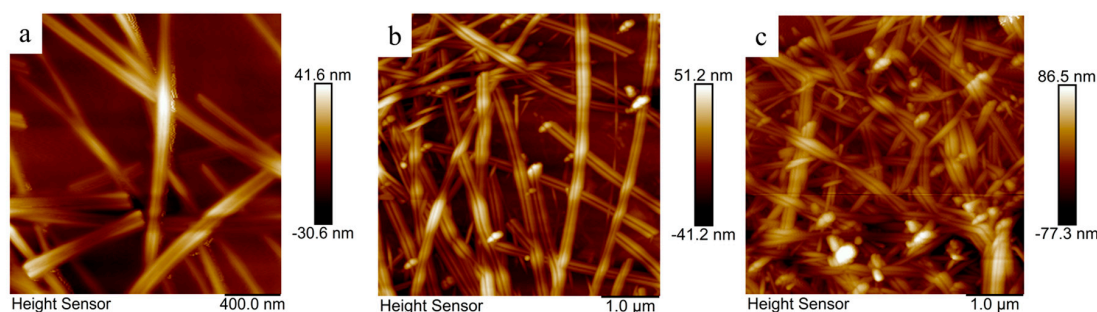


Figure 10. AFM images of films with AgNWs lengths of (a) 15.5 μm, (b) 9.24 μm, and (c) 7.86 μm.

Haze is defined as the ratio of diffuse transmittance to total transmittance according to ISO 14782 [37,38]. Figure 11a,b show the relationships between the haze of the film and the average AgNWs length of and film transmittance at 550 nm, respectively. The haze increases in the range 0.95–1.03% with decreasing in AgNWs length from 15.49 to 7.86 μm; these haze values are lower than those reported in the literature [19] and identical to that of ITO films. This was attributed to the smaller diameter of AgNWs used in our experiments and low RMS values of the films, which suppressed light scattering. Comparing the haze of films of AgNWs with the same diameter and different lengths revealed that haze slightly increased with decreasing AgNW length, which may be caused by the increasing deposition density of AgNWs on the substrate and number of contact points between AgNWs. This trend is consistent with the results of reported theoretical and experimental investigations [37]. It is worth noting that the film consisting of AgNWs with a length of 15.5 μm exhibited haze of 0.95%, transmittance of 93.42%, and sheet resistance of 80.15 Ω·sq⁻¹ without post-treatment. This performance is acceptable for use of the film in display devices.

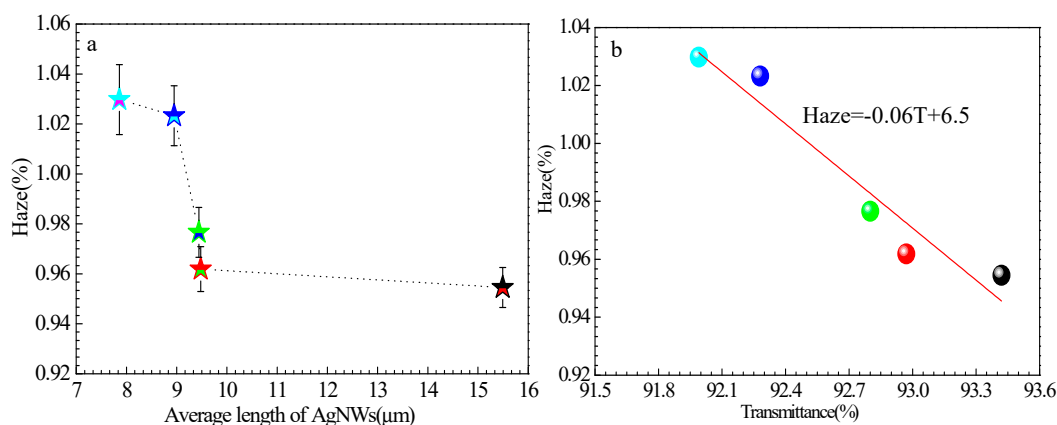


Figure 11. Relationship between the haze of AgNW-FTCFs and (a) the average AgNWs length and (b) transmittance at 550 nm.

After linear fitting of the data points plotted on a logarithmic scale, the following relationship between the haze and transmittance was found:

$$\text{Haze} = -0.06T + 6.5 \quad (4)$$

To demonstrate the applicability of the AgNW films, we connected green and blue LEDs to the conductive film, as shown in Figure 12. Figure 12a–c present photographs in which the device is flat, bent outward, and bent inward. In each case, the two LEDs work normally regardless of the bending state of the conductive AgNW film.

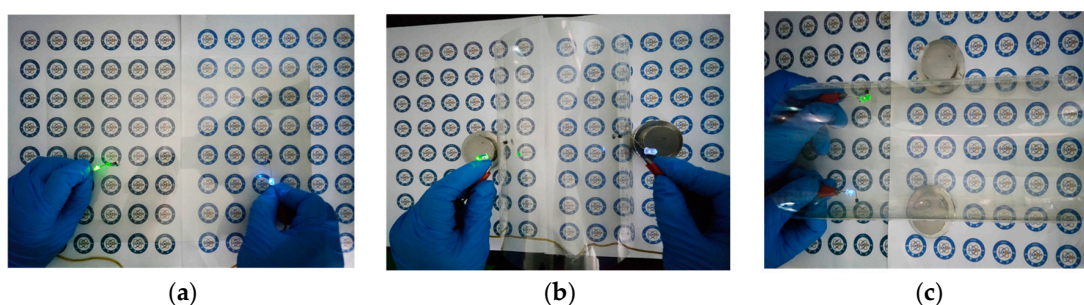


Figure 12. Photographs of devices containing green and blue LEDs the AgNWs film operating when (a) flat, (b) bent outward, and (c) bent inward.

3. Materials and Methods

3.1. Materials

An AgNW suspension was purchased from Suzhou Gushi New Materials Co., Ltd., Suzhou, China. The suspension contained AgNWs with an average diameter and length of 25 nm and 15.49 μm, respectively, dispersed in isopropyl alcohol at a concentration of 10 mg·mL⁻¹. Polyethylene terephthalate (PET) substrates were purchased from Hefei Microcrystalline Materials Co., Ltd., China. Ethanol absolute (99.7%) was purchased from Jinan Liyang Chemical Co., Jinan, Ltd., China. All the chemicals were used as received.

3.2. Sonication-Induced Scission of Silver Nanowires

For ultrasonication treatments, the AgNWs suspension was diluted to 2 mg·mL⁻¹ with isopropyl alcohol and then subjected to ultrasonication for 0.5–3 h at a power of 300 W. The ultrasonication was carried out in a bath-type sonicator (JP-120ST, 0–600 W, 28/40 kHz, Shenzhen Jiemeng Cleaning Equipment Co., Ltd., Shenzhen, China).

3.3. Fabrication of Flexible Transparent Conductive Silver Nanowires Film

AgNWs films were fabricated on PET substrates using a Mayer bar (No.7, R.D. Specialties Co., Ltd., Dallas, Texas, USA) and AgNWs suspension ($1.7 \text{ mg}\cdot\text{mL}^{-1}$) films were then dried in the ambient environment for 15 min.

3.4. Characterization

The size of the AgNWs was statistically characterized by scanning electron microscope (SEM; Zeiss Sigma 500, Carl Zeiss, Oberkochen, Germany). The lengths of individual AgNWs visible in the images were measured manually using image processing software (ImageJ, version 1.38, National Institutes of Health Bethesda, MD, USA). For one sample, we obtained six SEM images. The lengths of individual AgNW in the SEM image were measured manually according to an image processing software. The number of AgNW measured for each sample should not be less than 80. The sheet resistances of films were characterized using a four-probe system (ST2253, Suzhou Jingge Electronic Co., Ltd., Suzhou, China) and optical transmittances were measured using a thin film transmittance meter (GZ502A, Shanghai Guangzhao Optoelectronic Technology Co., Ltd., Shanghai, China). Diffuse reflectance was measured with an ultraviolet-visible spectrophotometer (760CRT, Shimadzu Ltd., Kuwabaracho, Japan). Optical transmittance and sheet resistance of AgNW-FTCFs were measured at 20 different sites, from which average values were calculated. The transmission and diffuse reflectance were measured using a PET film as a reference. The surface morphology was analyzed via atomic force microscopy (Dimension Edge, Bruker, Billerica, MA, USA).

4. Conclusions

AgNWs with an average diameter of about 25 nm and a length of 3.92–15.49 μm were obtained by sonication-induced scission. AgNW-FTCFs were then prepared on PET substrates and dried in the ambient environment. The film contains AgNWs with lengths of 5.17 and 3.92 μm were non-conductive because of the poor contact between the AgNWs. The sheet resistance and *NUF* of the AgNW-FTCFs increased by about 6400% and 178%, respectively, as the AgNWs length decreased from 15.5 to 7.86 μm . These results indicated that the distribution uniformity of AgNWs on the PET surface decreased as the ANW length shortened. The transmittance of the film at 500 nm decreased slightly from 93.42% to 91.99% and haze increased from 0.95% to 1.03% as the AgNWs length decreased from 15.49 to 7.86 μm . RMS values of the films were low (close to the diameter of a nanowire). The film consisting of AgNWs with a length of 15.5 μm exhibited haze of 0.95%, transmittance of 93.42%, and sheet resistance of $80.15 \Omega\cdot\text{sq}^{-1}$ without any additional post-treatment. These highly uniform and mechanically stable AgNW-FTCFs meet the requirement for numerous applications and could soon play a major role in the display market

Author Contributions: Y.W., X.Y., and X.Z. conceived and designed the experiments; X.Y., D.D., and Z.Y. performed the experiments and analyzed the data; Y.W. and Y.Z. contributed reagents/materials/analysis tools; and Y.W. wrote the paper. All authors have read and approved the final manuscript.

Funding: This work was financially supported by the National Science Foundation of China (61302044 and 61671140) and Zhongshan Science and Technology Projects (2018SYF10).

Conflicts of Interest: The authors declare no conflict of interest.

References

1. Wang, P.; Peng, Z.; Li, M. Stretchable Transparent conductive films from long carbon nanotube metals. *Small* **2018**, *14*. [[CrossRef](#)] [[PubMed](#)]
2. Chen, W.C.; Lien, H.T.; Cheng, T.W.; Su, C.; Chong, C.W.; Ganguly, A.; Chen, K.H.; Chen, L.C. Side group of poly(3-alkylthiophene)s controlled dispersion of single-walled carbon nanotubes for transparent conducting Film. *ACS Appl. Mater. Interfaces* **2015**, *7*, 4616–4622. [[CrossRef](#)] [[PubMed](#)]

3. Singh, B.P.; Nayak, S.; Nanda, K.K.; Singh, A.; Takai, C.; Takashi, S.; Fuji, M. Transparent, flexible, and conducting films based on graphene–polymer composites. *Polym. Compos.* **2018**, *39*, 297–304. [[CrossRef](#)]
4. Miao, J.L.; Liu, H.H.; Li, W.; Zhang, X. Mussel-inspired polydopamine-functionalized graphene as a conductive adhesion promoter and protective layer for silver nanowire transparent electrodes. *Langmuir* **2016**, *32*, 5365–5372. [[CrossRef](#)] [[PubMed](#)]
5. Kim, S.; Kim, B.; Im, I.; Kim, D.; Lee, H.; Nam, J.; Chung, H.K.; Lee, H.J.; Cho, S.M. Employment of gold-coated silver nanowires as transparent conductive electrode for organic light emitting diodes. *Nanotechnology* **2017**, *28*, 345201. [[CrossRef](#)] [[PubMed](#)]
6. Yu, Y.; Shen, W.; Li, F.; Fang, X.; Duan, H.; Xu, F.; Xiong, Y.; Xu, W.; Song, W. Solution-processed multifunctional transparent conductive films based on long silver nanowires/polyimide structure with highly thermostable and antibacterial properties. *RSC Adv.* **2017**, *7*, 28670–28676. [[CrossRef](#)]
7. Park, J.; Han, D.; Choi, S.; Kim, Y.; Kwak, J. Flexible transparent film heaters using a ternary composite of silver nanowire, conducting polymer, and conductive oxide. *RSC Adv.* **2019**, *9*, 5731–5737. [[CrossRef](#)]
8. Zhang, Y.; Guo, J.; Xu, D.; Sun, Y.; Yan, F. One-pot synthesis and purification of ultralong silver nanowires for flexible transparent conductive electrodes. *ACS Appl. Mater. Interfaces* **2017**, *9*, 25465–25473. [[CrossRef](#)] [[PubMed](#)]
9. Li, B.; Ye, S.R.; Stewart, I.E.; Alvarez, S.; Wiley, B.J. Synthesis and purification of silver nanowires to make conducting films with a transmittance of 99%. *Nano Lett.* **2015**, *15*, 6722–6726. [[CrossRef](#)] [[PubMed](#)]
10. Kumar, D.; Stoichkow, V.; Brousseau, E.; Smith, G.C.; Kettle, J. High performing AgNW transparent conducting electrodes with a sheet resistance of $2.5 \Omega \cdot \text{sq}^{-1}$ post-processing technique. *Nanoscale* **2019**, *11*, 5760–5769. [[CrossRef](#)] [[PubMed](#)]
11. Tang, L.; Zhang, J.; Dong, L.; Pan, Y.; Yang, C.; Li, M.; Ruan, Y.; Ma, J.; Lu, H. Coating-free, air-stable silver nanowires for high-performance transparent conductive film. *Nanotechnology* **2018**, *29*, 375601. [[CrossRef](#)] [[PubMed](#)]
12. Lv, P.; Zhou, H.; Zhao, M.; Li, D.; Lu, K.; Wang, D.; Huang, J.; Cai, Y.; Lucia, L.A.; Wei, Q. Highly flexible, transparent, and conductive silver nanowire attached bacterial cellulose conductors. *Cellulose* **2018**, *25*, 3189–3196. [[CrossRef](#)]
13. Liu, X.; Li, D.; Chen, X.; Lai, W.Y.; Huang, W. Highly transparent and flexible all-solid-state supercapacitors based on ultra-long silver nanowire conductive networks. *ACS Appl. Mater. Interfaces* **2018**, *10*, 32536–32542. [[CrossRef](#)] [[PubMed](#)]
14. Leem, D.S.; Edwards, A.; Faist, M.; Nelson, J.; Bradley, D.D.C.; Mello, J.C. Efficient organic solar cells with solution-processed silver nanowire electrodes. *Adv. Mater.* **2011**, *23*, 4371–4375. [[CrossRef](#)] [[PubMed](#)]
15. Xu, W.; Zhong, L.; Xu, F.; Shen, W.; Song, W.; Chou, S. Silver nanowire-based flexible transparent composite film for curvature measurement. *ACS Appl. Nano Mater.* **2018**, *1*, 3859–3866. [[CrossRef](#)]
16. Liu, R.; Tan, M.; Zhang, X.; Xu, L.; Chen, J.; Chen, Y.; Tang, X.; Wan, L. Solution-processed composite electrodes composed of silver nanowires and aluminum-doped zinc oxide nanoparticles for thin-film solar cells applications. *Sol. Energy Mater. Sol. Cells* **2018**, *174*, 584–592. [[CrossRef](#)]
17. Li, Y.; Yuan, X.; Yang, H.; Chao, Y.; Guo, S.; Wang, C. Solvothermal synthesis of ultra-fine silver nanowires with a diameter about 20 nm and an aspect ratio approximately 2000 for highly conductive flexible transparent film. *J. Mater. Sci. Mater. Electron.* **2019**, *30*, 8883–8891. [[CrossRef](#)]
18. Lagrange, M.; Langley, D.P.; Giusti, G.; Jiménez, C.; Bréchet, Y.; Bellet, D. Optimization of silver nanowire-based transparent electrodes: Effects of density, size and thermal annealing. *Nanoscale* **2015**, *7*, 17410–17423. [[CrossRef](#)]
19. Menampambath, M.M.; Yang, K.; Kim, H.H.; Bae, O.S.; Jeong, M.S.; Choi, J.-Y.; Baik, S. Reduced haze of transparent conductive films by smaller diameter silver nanowires. *Nanotechnology* **2016**, *27*, 465706. [[CrossRef](#)]
20. Preston, C.; Xu, Y.; Han, X.; Munday, J.N.; Hu, L. Optical haze of transparent and conductive silver nanowire films. *Nano Res.* **2013**, *6*, 461–468. [[CrossRef](#)]
21. Araki, T.; Jiu, J.; Nogi, M.; Koga, H.; Nagao, S.; Sugahara, T.; Suganuma, K. Low haze transparent electrodes and highly conducting air dried films with ultra-long silver nanowires synthesized by one-step polyol method. *Nano Res.* **2014**, *7*, 236–245. [[CrossRef](#)]

22. Chen, C.; Zhao, Y.; Wei, W.; Tao, J.; Lei, G.; Jia, D.; Wan, M.; Li, S.; Ji, S.; Ye, C. Fabrication of silver nanowire transparent conductive films with an ultra-low haze and ultra-high uniformity and their application in transparent electronics. *J. Mater. Chem. C* **2017**, *5*, 2240–2246. [[CrossRef](#)]
23. Bergin, S.M.; Chen, Y.H.; Rathmell, A.R.; Charbonneau, P.; Li, Z.Y.; Wiley, B.J. The effect of nanowire length and diameter on the properties of transparent, conducting nanowire films. *Nanoscale* **2012**, *4*, 1996–2004. [[CrossRef](#)] [[PubMed](#)]
24. Sorel, S.; Lyons, P.E.; De, S.; Dickerson, J.C.; Coleman, J.N. The dependence of the optoelectrical properties of silver nanowire networks on nanowire length and diameter. *Nanotechnology* **2012**, *23*, 185201. [[CrossRef](#)] [[PubMed](#)]
25. Ramadhan, Z.R.; Han, J.W.; Lee, D.J.; Entifar, S.A.N.; Hong, J.; Yun, C.; Kim, Y.H. Surface-functionalized silver nanowires on chitosan biopolymers for highly robust and stretchable transparent conducting films. *Mater. Res. Lett.* **2019**, *7*, 124–130. [[CrossRef](#)]
26. Jia, Y.G.; Chen, C.; Jia, D.; Li, S.X.; Ji, S.L.; Ye, C.H. Silver nanowire transparent conductive films with high uniformity fabricated via a dynamic heating method. *ACS Appl. Mater. Interfaces* **2016**, *8*, 9865–9871. [[CrossRef](#)]
27. Zhang, C.P.; Zhu, Y.W.; Yi, P.Y.; Peng, L.F.; Lai, X.M. Fabrication of flexible silver nanowire conductive films and transmittance improvement based on moth-eye nanostructure array. *J. Micromech. Microeng.* **2017**, *27*, 075010. [[CrossRef](#)]
28. Kim, S.; Jeon, H.R.; An, C.H.; An, B.S.; Yang, C.W.; Lee, H.J.; Weon, B.M. Improvement of conductivity of Ag nanowires-networked film using 1,8-diazabicyclo[5,4,0]undec-7-ene (DBU). *Mater. Lett.* **2017**, *193*, 63–66. [[CrossRef](#)]
29. Zong, R.L.; Zhou, J.; Li, Q.; Du, B.; Li, B.; Fu, M.; Qi, X.W.; Li, L.T. Synthesis and optical properties of silver nanowires arrays embedded in anodic alumina membrane. *J. Phys. Chem. B* **2004**, *108*, 16713–16716. [[CrossRef](#)]
30. Elsner, H.I.; Lindblad, E.B. Ultrasonic degradation of DNA. *DNA* **1989**, *8*, 697–701. [[CrossRef](#)]
31. Marus, M.; Hubarevich, A.; Lim, R.J.W.; Huang, H.; Smirnov, A.; Wong, H.; Fan, W.J.; Sun, X.W. Effect of silver nanowire length in a broad range on optical and electrical properties as a transparent conductive film. *Opt. Mater. Express* **2017**, *7*, 1105–1112. [[CrossRef](#)]
32. Yang, X.; Du, D.X.; Wang, Y.H. Length-dependent electro-optical properties of silver nanowires-based transparent conducting films. *J. Mater. Sci. Mater. Electron.* **2019**, *30*, 6838–6845. [[CrossRef](#)]
33. Zheng, B.; Zhu, Q.; Zhao, Y. Flexible silver nanowire transparent conductive films prepared by an electrostatic adsorption self-assembly process. *J. Mater. Sci.* **2019**, *54*, 5802–5812. [[CrossRef](#)]
34. Hwang, H.J.; Malhotra, R. Shape-Tuned Junction Resistivity and Self-Damping Dynamics in Intense Pulsed Light Sintering of Silver Nanostructure Films. *ACS Appl. Mater. Interfaces* **2019**, *11*, 3536–3546. [[CrossRef](#)] [[PubMed](#)]
35. Anoshkin, I.V.; Nefedova, I.I.; Nefedov, I.S.; Lioubtchenko, D.V.; Nasibulin, A.G.; Räisänen, A.V. Resistivity and optical transmittance dependence on length and diameter of nanowires in silver nanowire layers in application to transparent conductive coatings. *Micro Nano Lett.* **2016**, *11*, 343–347. [[CrossRef](#)]
36. Yip, H.L.; Jen, A.K.Y. Recent advances in solution-processed interfacial materials for efficient and stable polymer solar cells. *Energy Environ. Sci.* **2012**, *5*, 5994–6011. [[CrossRef](#)]
37. Khanarian, G.; Joo, J.; Liu, X.-Q.; Eastman, P.; Werner, D.; Connell, K.; Trefonas, P. The optical and electrical properties of silver nanowire mesh films. *J. Appl. Phys.* **2013**, *114*, 024302. [[CrossRef](#)]
38. Menampambath, M.M.; Muhammed, A.C.; Kim, K.H.; Yang, D.; Roh, J.; Park, H.C.; Kwak, C.; Choi, J.-Y.; Baik, S. Silver nanowires decorated with silver nanoparticles for low-haze flexible transparent conductive films. *Sci. Rep.* **2015**, *5*, 16371. [[CrossRef](#)] [[PubMed](#)]

